Rare Metal Materials and Engineering
Volume 51, Issue 1, January 2022
Available online at www.rmme.ac.cn

Science Press

Cite this article as: Luo Ning, Sun Xin, Fan Xueru, et al. Controllable Synthesis of Polycrystalline Nanostructure TiO_2 by Gaseous-Liquid Detonation Method[J]. Rare Metal Materials and Engineering, 2022, 51 (01): 119-126.

ARTICLE

Controllable Synthesis of Polycrystalline Nanostructure TiO_2 by Gaseous-Liquid Detonation Method

Luo Ning[1,2,3], Sun Xin[1,2,3], Fan Xueru[1,2], Liang Hanliang[1,2,3], Chen Yanlong[1,2], Zhang Guimin[1,2], Dong Jiwei[1,2], Zhai Cheng[4]

[1] School of Mechanics and Civil Engineering, China University of Mining and Technology, Xuzhou 221116, China; [2] State Key Laboratory for Geomechanics and Deep Underground Engineering, China University of Mining and Technology, Xuzhou 221116, China; [3] Explosive Mechanics and Engineering Blasting Research Center, China University of Mining and Technology, Xuzhou 221116, China; [4] School of Safety Engineering, China University of Mining and Technology, Xuzhou 221116, China

Abstract: The polycrystalline nano-TiO_2 was synthesized by the gaseous-liquid detonation (GLD) method using H_2, O_2, and $TiCl_4$ as the mixture precursors. The effects of different molar ratios of precursors and initial reaction pressures on the nano-TiO_2 crystalline structures were studied. The nanocrystal structures, components, particle size, and morphology were characterized by the X-ray diffraction (XRD) and transmission electron microscopy (TEM). The results demonstrate that the nano-TiO_2 consists of pure anatase-TiO_2, pure rutile-TiO_2, and the mixtures of spherical or quasi-spherical morphologies with particle size of 20~150 nm. Furthermore, the formation mechanism of nano-TiO_2 by GLD method was analyzed. The relevant GLD parameters were calculated based on the C-J theory and the related chemical reaction data, which effectively verifies the influence of different molar ratios of precursors and initial pressures on the controllable synthesis of polycrystalline nano-TiO_2.

Key words: nano-TiO_2; gaseous-liquid detonation; polycrystalline nanostructure; detonation parameters; C-J theory

Nano-TiO_2 is one of the most extensively used nanomaterials due to its stable chemical structure, biocompatibility, and physical, optical, and electrical properties, and it is normally used in catalysis[1-3], Li-ion batteries[4-6], gas sensors[7,8], and antibacterial active materials[9,10]. Generally, the TiO_2 crystals have three polymorphic phases: anatase, rutile, and brookite. The anatase and rutile are two important structures of TiO_2 used in commercial products[11]. The pure nano-TiO_2 is often prepared by hydrothermal synthesis, flame method, and chemical vapor deposition (CVD) method. Hydrothermal method can synthesize different TiO_2 nanocrystals under the hydrothermal environment. Lin et al[12] fabricated a series of mixed-phases of TiO_2 by hydrothermal synthesis using $TiCl_3$ as the precursor and ammonia water for regulating the ratio of different crystal phases. Flame method can adjust the component, size, and morphology of nanomaterials. Wu et al[13] explored the transformation of nano-TiO_2 crystal phase and fabricated pure anatase-TiO_2 by changing the flame gas flow rates of the fuel, oxygen, and argon carrier. CVD method is widely used to prepare nano-TiO_2, because it can easily control the crystal type and morphology by adjusting the gas ratio and dosage of catalyst. Chen et al[14] reported that rutile-TiO_2 nanowires are grown on the Ti foil through controlling the growth temperature and the thickness of the catalyst layer which is important for activating the surface of Ti foil and facilitating the TiO_2 growth in CVD system.

However, these conventional techniques require long time for production and advanced equipment. Compared with these techniques, the gaseous-liquid detonation (GLD) method has its unique advantages of simple operation and provides the high temperature and high pressure conditions for rapid reaction and growth of nanomaterials[15-17]. Luo et al[18,19] used H_2, O_2, C_2H_6O, and $TiCl_4$ as the precursors to prepare TiO_2 and discussed the growth of spherical TiO_2 during rapid detonation reaction process. Wu et al[20,21] synthesized SnO_2-TiO_2

Received date: January 19, 2021
Foundation item: National Natural Science Foundation of China (12072363); National Key Research and Development Project (2020YFA0711800)
Corresponding author: Luo Ning, Ph. D., Professor, School of Mechanics and Civil Engineering, China University of Mining and Technology, Xuzhou 221116, P. R. China, E-mail: nluo@cumt.edu.cn

nanocomposites and nano-Fe_2O_3-TiO_2 composites by detonation method, and investigated the influence of Sn^{4+} and Fe^{3+} on the crystalline structure of nano-TiO_2. Nevertheless, the synthesis mechanism of crystalline structure of nano-TiO_2 is still unclear, which greatly restricts its industrial production.

In this research, different nano-TiO_2 crystals were prepared by GLD method through adjusting the precursor (H_2, O_2, $TiCl_4$, and C_2H_6O) content and initial pressure. The X-ray diffraction (XRD) and transmission electron microscopy (TEM) were used to characterize the crystalline structure, components, particle size, and morphology of nano-TiO_2. Furthermore, by combining C-J theory with chemical reaction data, different crystalline structures of nano-TiO_2 were analyzed.

1 Experiment

The polycrystalline nano-TiO_2 was prepared in the GLD system, as shown in Fig. 1. The GLD tube consisted of two modules with different lengths, namely the deflagration module of 0.5 m in length and the detonation tube module of 1.5 m in length. The shock tube was made of titanium alloy and the inner diameter was 0.1 m.

In a typical preparation procedure, the GLD tube was heated to 380~550 K after vacuuming (barometer reading-0.09 MPa). A certain amount of $TiCl_4$ solution was injected by the atomizer into the tube. Then the mixed gas with a certain proportion of H_2 and O_2 was pumped into the GLD synthesis system until reaching the atmosphere pressure. The gaseous-liquid mixtures were placed statically for 5~10 min and then ignited using the electric igniter of 20~40 J. Finally, after the tube was cooled down to room temperature, the white products were collected from the inner wall of GLD tube and washed with absolute ethanol.

The nano-TiO_2 phases and crystalline structure of the detonation products were characterized by D/MAX 2400 XRD (Cu Kα, λ=0.154 06 nm). The tube voltage was 40 kV, the tube current was 30 A, and the scanning range was 20°~80°. The morphologies of nano-TiO_2 structure were observed using TEM (Tecnai F30, FEI) with point resolution of 0.2 nm and line resolution of 0.1 nm.

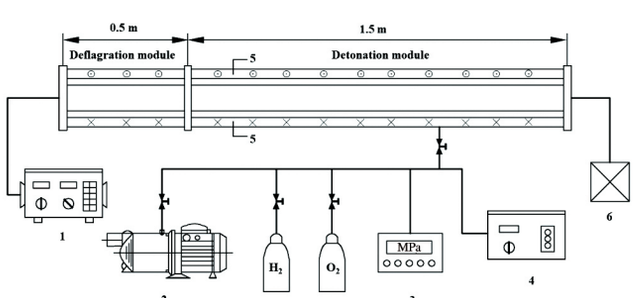

1-high energy igniter; 2-vacuum pump; 3-barometer; 4-liquid atomizing system; 5-temperature control system; 6-exhaust gas treatment equipment

Fig.1 Schematic diagram of GLD system

2 Calculation of GLD Parameters

The gaseous-liquid mixture precursors consisted of gas mixture and $TiCl_4$ was ignited by the high energy spark of 20~40 J to prepare nano-TiO_2. During the GLD process, the detonation heat, high temperature, and high pressure were generated, resulting in the fact that the mixture precursors decompose into nano-TiO_2. The related chemical reactions are as follows:

$$2H_2(g) + O_2(g) = 2H_2O(g) \quad (1)$$

$$TiCl_4(g) + 2H_2O(g) = TiO_2(s) + 4HCl(g) \quad (2)$$

When the chemical equilibrium was attained, a steady-state detonation was achieved and its propagation rate was governed only by the thermodynamics and hydrodynamics. Assuming that a standing detonation wave is similar to the calculated shock waves, the laws of conservation of mass, momentum, and energy applied across the shock front may lead to the conservation equations[18], as follows:

$$\rho_0(D_0 - u_0) = \rho_{CJ}(D_{CJ} - u_{CJ}) \quad (3)$$

$$P_0 + \rho_0(D_0 - u_0)^2 = P_{CJ} + \rho_{CJ}(D_{CJ} - u_{CJ})^2 \quad (4)$$

$$e_0 + \frac{P_0}{\rho_0} + \frac{(D_0 - u_0)^2}{2} = e_{CJ} + \frac{P_{CJ}}{\rho_{CJ}} + \frac{(D_{CJ} - u_{CJ})^2}{2} + Q \quad (5)$$

$$\frac{P_{CJ} - P_0}{V_0 - V_{CJ}} = \gamma \frac{P_{CJ}}{V_{CJ}} \quad (6)$$

where ρ is the gas density, D is the detonation velocity, u is the particle velocity, P is the detonation pressure, e is the specific internal energy, Q is the released specific heat from explosions, γ is the isentropic adiabatic index exponent, V is the ideal gas volume, and the subscript 0 and CJ represent the physical quantities before and after rapid reaction, respectively. Internal energy e_i can be expressed by Eq.(7), as follows:

$$e_i = \frac{P_i V_i}{\gamma_i - 1} \quad i = 0 \text{ or CJ} \quad (7)$$

Assuming that $\gamma_0 = \gamma_{CJ} = \gamma$, $P_0 \ll P_{CJ}$, the results can be calculated according to Eq.(8~11), as follows:

$$D = \sqrt{2(\gamma^2 - 1)Q} \quad (8)$$

$$P_{CJ} = \frac{\rho_0 D^2}{\gamma + 1} \quad (9)$$

$$\rho_{CJ} = \frac{\gamma + 1}{\gamma}\rho_0 \quad (10)$$

$$u_{CJ} = \frac{D}{\gamma + 1} \quad (11)$$

The calculation of gaseous detonation heat is based on Hess's law of thermochemistry. According to the first law of thermodynamics, the relationship between thermal effect at constant volume Q_V and constant thermal effect Q_P can be expressed by Eq.(12), as follows:

$$Q_V = Q_P + P(V_j - V_i) \quad (12)$$

where V_i and V_j refer to the volume content of gas before and after the reaction, respectively. Assuming that the gas temperature T is constant before and after detonation reaction, the equation of the state of prefect gas can be obtained as

Eq.(13), as follows:

$$P(V_j - V_i) = (n_j - n_i)RT \quad (13)$$

where R is the constant of the perfect gas, and n_i and n_j refer to the molar content of gas before and after the reaction, respectively. Q_P after detonation can be calculated by the enthalpy increase of the system, as expressed by Eq.(14):

$$Q_P = \sum n_j \Delta H_{fj}^0 - \sum n_i \Delta H_{f,i}^0 \quad (14)$$

where ΔH_{fj}^0 and $\Delta H_{f,i}^0$ are standard molar enthalpies of detonation products and precursors, respectively. Assuming that the heat capacity at constant pressure C_V is only a function of temperature T, according to laws of thermodynamics, the detonation heat at constant pressure can be expressed by Eq.(15):

$$Q_V = \int_{T_i}^{T_j} C_V \mathrm{d}T = t\overline{C}_V = (T_j - T_i)\sum n_j \overline{C}_{V,j} \quad (15)$$

where T_j is the detonation temperature; T_i is the initial temperature; t is the temperature difference before and after detonation; $C_{V,j}$ is the average molecular thermal capacity at constant volume for detonation products. $C_{V,j}$ can also be expressed by Eq.(16), as follows:

$$\overline{C}_{V,j} = a_j + b_j t \quad (16)$$

where a_j and b_j are the molecular constant volume heat capacity of detonation reaction product components. For C_V of all the detonation products, it can be summarized according to Eq.(17):

$$\overline{C}_V = A + Bt \quad (17)$$

where $A = \sum n_j a_j$ and $B = \sum n_j b_j$. Substituting Eq. (16) and Eq. (17) into Eq. (15), the detonation temperature can be obtained, as expressed by Eq.(18):

$$T_j - T_i = \frac{-A + \sqrt{A^2 + 4BQ_V}}{2B} \quad (18)$$

Table 1 shows the formation enthalpies of $TiCl_4$, TiO_2, H_2O, and HCl at different temperatures. Table 2 shows the calculation results or relationship of average molecular thermal capacity at constant volume of different substances.

Table 1 Standard formation enthalpies of $TiCl_4$, TiO_2, H_2O, and HCl (kJ/mol)[22]

Substance	400 K	500 K
$TiCl_4$	−762.843	−762.501
Anatase-TiO_2	−936.286	−937.439
Rutile-TiO_2	−944.364	−943.603
H_2O	−223.951	−219.951
HCl	−92.581	−92.907

Table 2 Calculation results and relationship of average molecular thermal capacity at constant volume ($J \cdot mol^{-1} \cdot K^{-1}$)[23]

Substance	C_V
Solid matter	24.9~25.4
Monatomic gas	20.77
Diatomic gas	20.0+0.001 88t
H_2O, H_2S	16.7+0.008 97t
CO_2, SO_2	37.5+0.002 42t

3 Results and Discussion

3.1 XRD analysis

Nineteen specimens were prepared under different conditions according to Table 3, and were named as S1~S19 in sequence.

The XRD patterns of prepared nano-TiO_2 products are shown in Fig. 2. The diffraction peaks at 2θ=25.3°, 37.8°, 48.0°, 53.9°, and 62.7° correspond to the anatase-TiO_2 (according to JCPDS No. 99-0008), and those at 2θ=27.4°, 36.0°, 41.2°, and 54.3° correspond to the rutile-TiO_2 (JCPDS No.99-0090). Therefore, it can be seen that all specimens have a mixed crystalline structure, except S9 and S13 which only possess rutile-TiO_2 phase. Fig. 2a shows XRD patterns of S1~S5 with preparation condition of O_2:H_2:$TiCl_4$=1.0:1.0~3.0:1.0, presenting an upward trend for anatase-TiO_2 content but a downtrend for rutile-TiO_2 content with increasing the H_2 content. Fig. 2b shows XRD patterns of S6~S9 with the preparation condition of O_2: H_2: $TiCl_4$=0.5~2.0: 2.0: 1.0, which have the similar trends of anatase-TiO_2 and rutile-TiO_2 contents with increasing the O_2 content, compared with those in Fig. 2a. Fig. 2c shows XRD patterns of S10~S13 with the preparation condition of O_2: H_2: $TiCl_4$=1.0: 2.0: 0.5~1.5. The increasing $TiCl_4$ content leads to the decline in anatase-TiO_2 production but results in the augmentation in rutile-TiO_2. Fig. 2d shows XRD patterns of S14~S16 with the preparation condition of O_2: H_2: $TiCl_4$=1.0~2.33: 2.0~4.66: 1.0. When the molar ratio of H_2 to O_2 is fixed and the $TiCl_4$ amount is unchanged, increasing initial pressure is conducive to the generation of rutile-TiO_2. Fig. 2e shows XRD patterns of S17~S19 with the preparation condition of O_2: H_2: $TiCl_4$=1.0: 2.0:0.5~1.5. The change trends of anatase-TiO_2 and rutile-TiO_2 contents are similar to those in Fig. 2c, but the nano-TiO_2 crystalline structure is slightly different on account of the discrepancy in initial temperature.

The average crystal size of nano-TiO_2 powder can be calculated by the Scherrer equation: $D=K\lambda/\beta\cos\theta$, where D is the average crystal size of grains, K is a constant of 0.89, λ represents the X-ray wavelength, β represents the half-peak width of the corresponding diffraction peak, and θ represents the Bragg angle of diffraction peaks. The calculated results of average crystal size of nano-TiO_2 powder are shown in Table 3.

The crystal content of anatase-TiO_2 and rutile-TiO_2 from gaseous detonation can be calculated by Spurr and Myers formula[24], as expressed by Eq.(19) and Eq.(20), respectively:

$$W_A = \frac{K_A I_A}{K_A I_A + I_R} \quad (19)$$

$$W_R = \frac{I_R}{K_A I_A + I_R} \quad (20)$$

where I_A represents the integrated intensity of the (101) peak of anatase-TiO_2, I_R represents the height of (110) peak of rutile-TiO_2, and K_A is a constant of 0.884. The calculated results are shown in Table 3.

Table 3 Preparation conditions, component proportions, and crystal sizes of S1~S19 specimens

Specimen	Initial temperature/K	Initial pressure/MPa	O_2:H_2:$TiCl_4$	Content/wt%		Crystal size/nm	
				Anatase	Rutile	Anatase	Rutile
S1	423	0.1	1.0:2.0:1.0	45.8	54.2	26	37
S2	423	0.1	1.0:3.0:1.0	76.9	23.1	42	22
S3	423	0.1	1.0:2.5:1.0	67.3	33.7	38	20
S4	423	0.1	1.0:1.5:1.0	28.1	71.9	44	44
S5	423	0.1	1.0:1.0:1.0	11.4	88.6	55	49
S6	423	0.1	2.0:2.0:1.0	86.8	13.2	49	63
S7	423	0.1	1.5:2.0:1.0	77.9	22.1	53	59
S8	423	0.1	0.75:2.0:1.0	5.7	94.3	33	35
S9	423	0.1	0.5:2.0:1.0	-	-	-	-
S10	423	0.1	1.0:2.0:0.5	50.8	49.2	47	53
S11	423	0.1	1.0:2.0:0.75	47.7	52.3	50	49
S12	423	0.1	1.0:2.0:1.25	35.7	64.3	56	54
S13	423	0.1	1.0:2.0:1.5	0.1	99.9	-	46
S14	413	0.1	1.0:2.0:1.0	57.4	42.6	13	34
S15	413	0.15	1.66:3.22:1.0	56.3	43.7	20	40
S16	413	0.2	2.33:4.66:1.0	24.8	75.2	35	40
S17	413	0.1	1.0:2.0:1.5	15.7	84.3	34	45
S18	413	0.1	1.0:2.0:1.25	23.1	76.9	26	31
S19	413	0.1	1.0:2.0:0.5	76.5	23.5	10	21

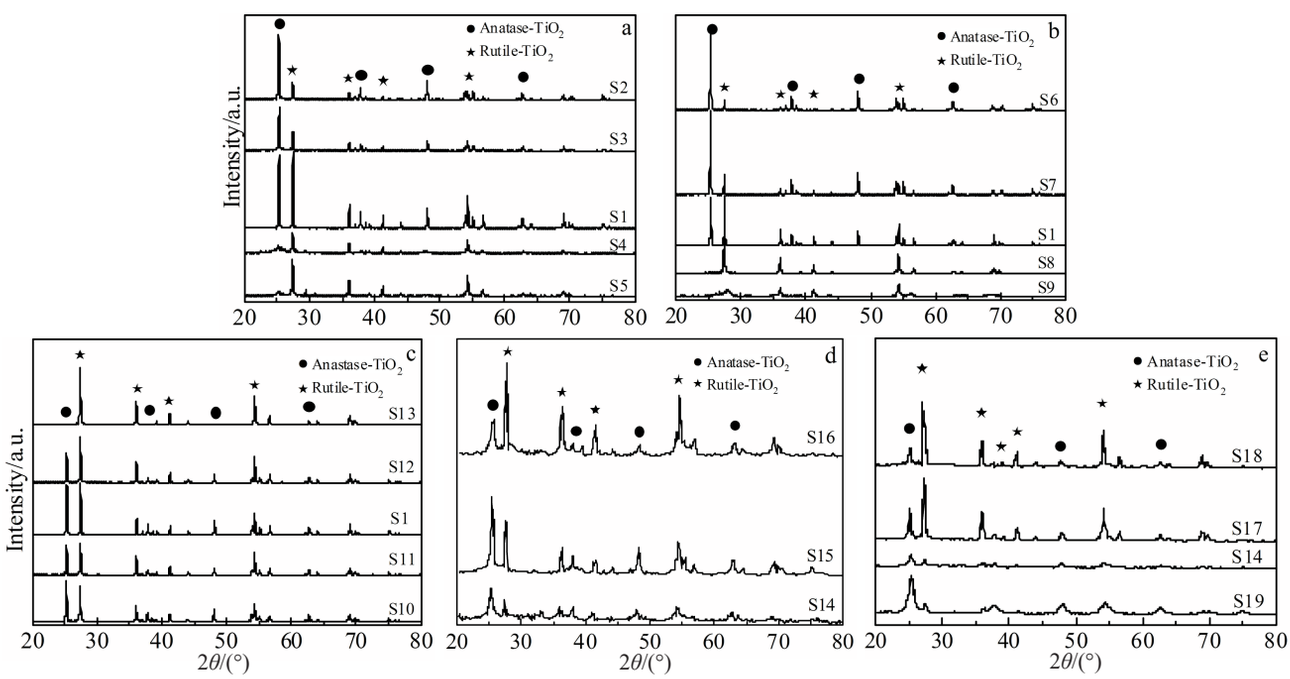

Fig.2 XRD patterns of S1~S5 (a), S6~S9 (b), S10~S13 (c), S14~S16 (d), and S17~S19 (e) specimens

3.2 TEM analysis

The microstructure of representative products S1, S6, and S13 was investigated by TEM, as shown in Fig. 3. It can be seen that the nano-TiO_2 of S1 specimen has mixture phases of 45.8wt% anatase-TiO_2 and 54.2wt% rutile-TiO_2. The products consist of spherical or quasi-spherical nanoparticles with particle size in a larger wide range of 20~150 nm. S6 specimen possesses good dispersity and relatively uniform crystal size of 40~60 nm. The main component of S6 specimen is anatase-TiO_2 (86.8wt%). It is also demonstrated that S13 specimen is pure rutile-TiO_2 and the average crystal size is 46 nm. The particle dispersity of S13 is relatively good,

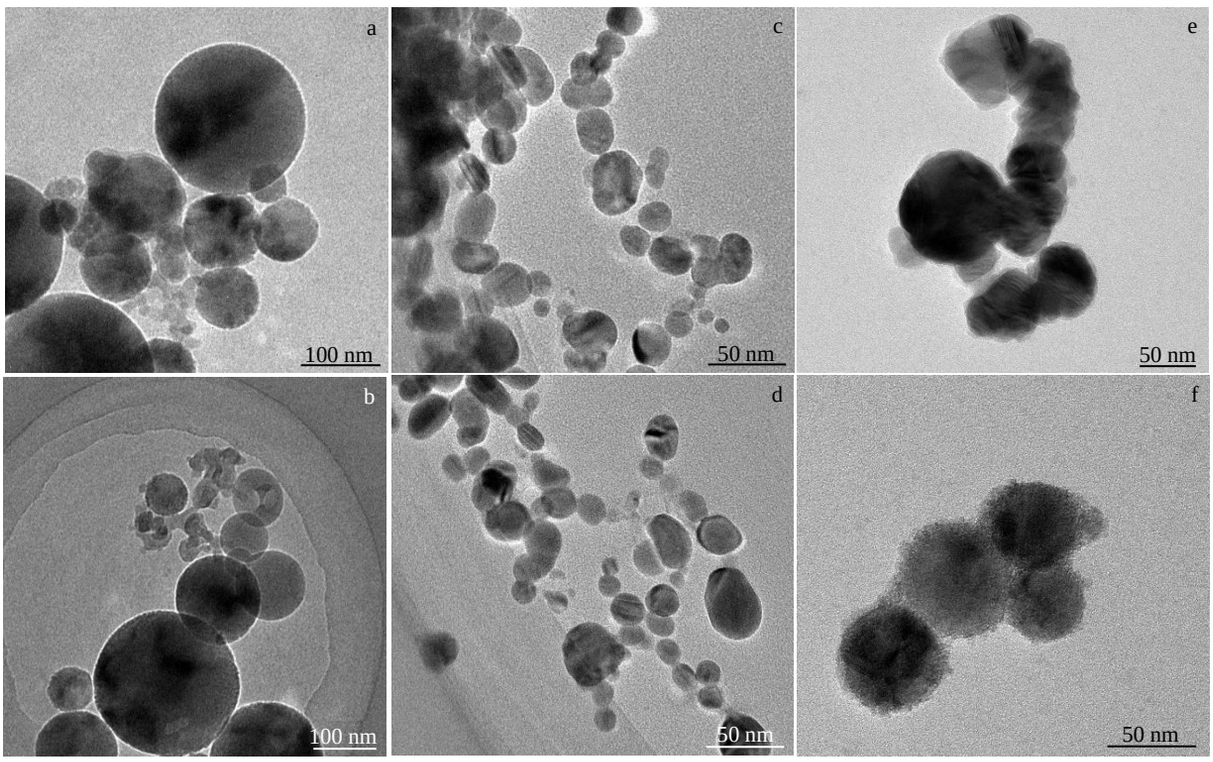

Fig.3 TEM images of S1 (a, b), S6 (c, d), and S13 (e, f) specimens

shows only a slight agglomeration.

3.3 Controllable synthesis of nano-TiO_2

Fig.4 shows the changing trend of anatase-TiO_2 content and rutile-TiO_2 content under different initial reaction conditions. Fig. 4a shows that with solely increasing the H_2 content, the content of anatase-TiO_2 and rutile-TiO_2 is increased and decreased, respectively. Fig. 4b shows that with solely increasing the O_2 content, the content of anatase-TiO_2 is also increased. Fig. 4c and 4e show that with solely increasing the $TiCl_4$ content, the rutile-TiO_2 phase is increased while the anatase-TiO_2 phase is decreased, i.e., the transformation from anatase-TiO_2 to rutile-TiO_2 is enhanced. With solely increasing the initial pressure of H_2/O_2, the generation of rutile-TiO_2 is increased, as shown in Fig. 4d. Compared with Fig. 4a and 4b, it can be seen that when the content of H_2 or O_2 exceeds the content of $TiCl_4$, the amount of anatase-TiO_2 is effectively increased.

During the GLD process, the leading shock wave flows through unreacted gas mixtures may cause a series of violent chemical reactions. The detonation heat under the atmosphere of high temperature and high pressure is generated rapidly during GLD chemical reaction. The GLD parameters were calculated based on the C-J theory, as shown in Table 4. The calculated results show that the maximum detonation parameters of detonation temperature, detonation pressure, and detonation velocity are 4271 K, 7.33 MPa, and 2946 m/s, respectively. The detonation condition for obtaining pure rutile-TiO_2 is detonation temperature of 3583 K, detonation pressure of 3.36 MPa, and detonation velocity of 1823 m/s. Under the atmosphere of instantaneous high temperature and high pressure, all the mixture precursors may decompose into ions and then form tiny TiO_2 which agglomerates to form nano-TiO_2 gradually[25]. The results of thermodynamic calculation show that the phase stability of rutile-TiO_2 and anatase-TiO_2 decreases generally, which depends on the difference of surface energy. As long as the crystal size is small enough, the stability of anatase phase is stable[26,27]. Zhao et al[28] reported that the critical diameter of anatase phase is less than that of rutile phase during the detonation reaction process, the crystal nucleus of anatase phase is generated at first, and the grains gradually grow. Hanaor et al[29] summarized that the transformation temperature is 400~1200 °C since the transformation temperature is determined by the raw materials and preparation methods. In addition, the conversion rate of anatase-TiO_2 to rutile-TiO_2 depends on time[30]. The transformation kinetics is related to the temperature-time conditions during the GLD chemical reaction. However, it is very difficult to measure the reaction and transformation time of preparation of nano-TiO_2 during the GLD process. Thus, the reaction and transformation time can only be simply determined by detonation velocity. The effects of two main reactions and cations on the transformation of anatase-TiO_2 to rutile-TiO_2 in the process of GLD reaction were discussed in Ref. [31]. The status under two important conditions need to be discussed: (1) the half content of water vapor from reaction of H_2 and O_2 is less than the content of $TiCl_4$; (2) the half content of water vapor is more than or equal to the content of $TiCl_4$.

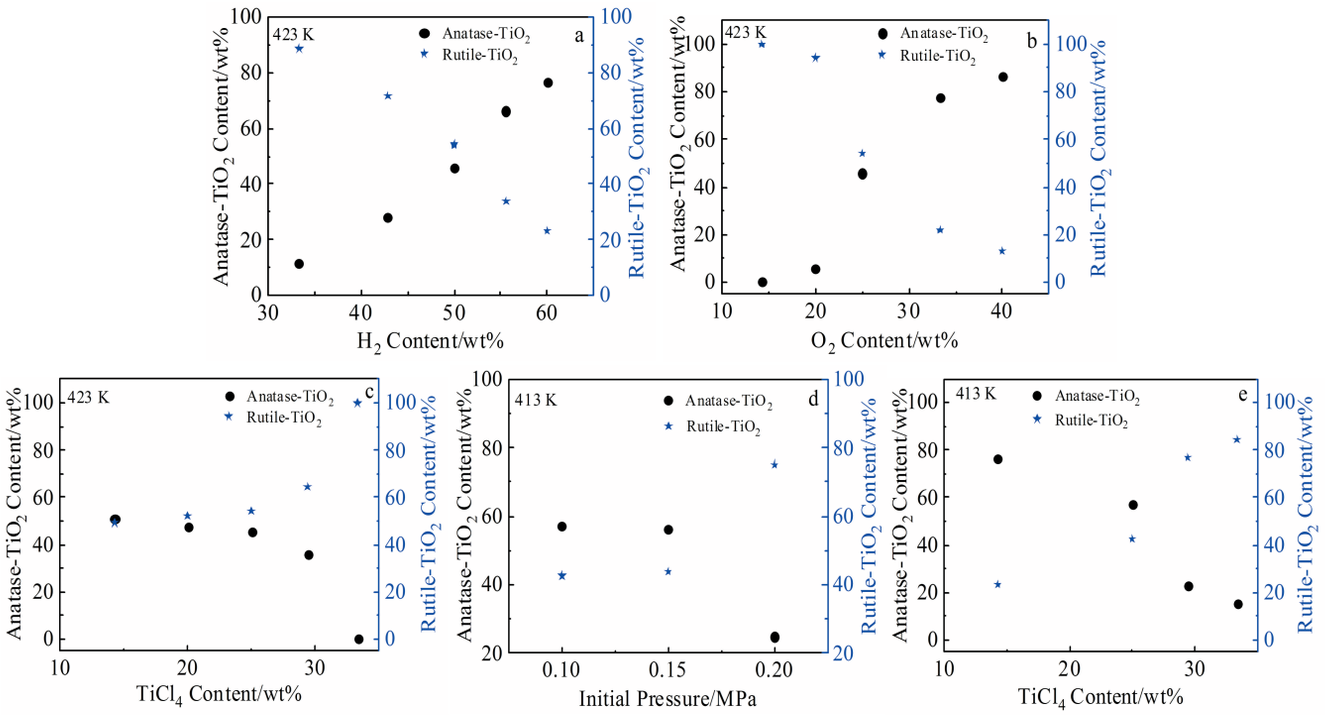

Fig.4 Influence of different initial reaction conditions on contents of anatase-TiO_2 and rutile-TiO_2: (a) H_2 content; (b) O_2 content; (c) $TiCl_4$ content at 423 K; (d) initial pressure; (e) $TiCl_4$ content at 413 K

Table 4 Calculated GLD parameters of S1~S19 specimens

Specimen	Detonation temperature/K	Detonation pressure/MPa	Detonation Velocity/m·s^{-1}	Content/wt%	
				Anatase	Rutile
S1	4135	3.91	2212	45.8	54.2
S2	3553	3.15	2207	76.9	23.1
S3	3820	3.49	2210	66.3	33.7
S4	3878	3.72	2021	28.1	71.9
S5	3543	3.46	1808	11.4	88.6
S6	3553	3.15	2075	86.8	13.2
S7	3820	3.49	2140	77.9	22.1
S8	3572	3.25	1984	5.7	94.3
S9	2862	2.49	1706	-	-
S10	4252	4.15	2801	50.8	49.2
S11	4195	4.02	2445	47.7	52.3
S12	3846	3.62	1993	35.7	64.3
S13	3583	3.36	1823	-	99.9
S14	4144	3.42	2218	57.4	42.6
S15	4234	5.37	2639	56.3	43.7
S16	4271	7.33	2946	24.8	75.2
S17	3854	3.17	1999	15.7	84.3
S18	3591	2.95	1829	23.1	76.9
S19	4256	3.63	2806	76.5	23.5

Fig. 5a shows the variation of rutile-TiO_2 content and detonation velocity with calculated temperature under the former condition. The results show that the content of rutile-TiO_2 by GLD method is related to detonation temperature and velocity. Initially, the content of rutile-TiO_2 is increased with increasing the detonation temperature. When the detonation

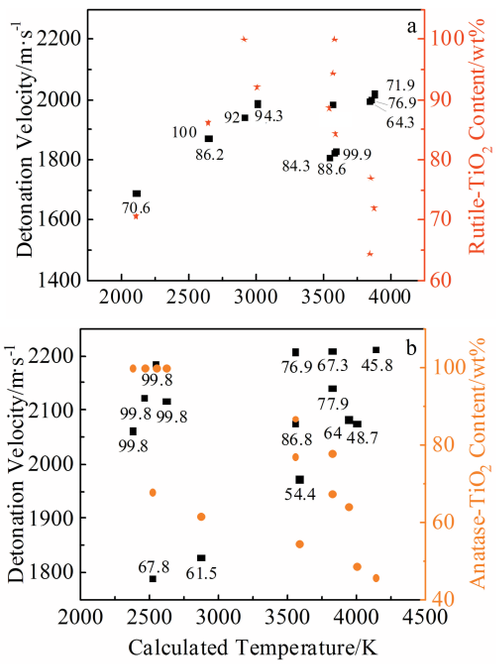

Fig.5 Variation of rutile-TiO_2 content and detonation velocity with calculated temperature under the former condition (a); variation of anatase-TiO_2 and detonation velocity with calculated temperature under the latter condition (b)

temperature is more than 3500 K, the content of rutile-TiO_2 products is reduced. It can be concluded that the rutile-TiO_2 of high purity is generated at detonation temperature of 3000~3500 K and the detonation velocity is 1800~2000 m/s under this condition. Fig.5b shows the variation of anatase-TiO_2 and detonation velocity with calculated temperature under the latter condition. The increasing temperature inhibits the formation of anatase-TiO_2, i.e., the formation of rutile-TiO_2 is promoted. On the other hand, when the alcohol solution is added into the mixture precursors (O_2:H_2:$TiCl_4$:C_2H_6O=1.0:2.0:1.0:0.3~0.6), the pure anatase-TiO_2 appears at temperature of 2400~2600 K and the detonation velocity is 2100~2200 m/s under this condition. The formation of pure anatase-TiO_2 is related to higher detonation velocity. During the GLD process, the transformation time of anatase-TiO_2 into rutile-TiO_2 is shortened, which is conducive to the formation of anatase-TiO_2, which is possibly related with the inhibitory effect of anion[29].

4 Conclusions

1) Nano-TiO_2 of different crystal structures have spherical or quasi-spherical shapes with good dispersity, and the crystal size is 20~150 nm.

2) Under the conditions of stable gaseous-liquid detonation (GLD), when the content of H_2 or O_2 exceeds that of $TiCl_4$, the production of anatase-TiO_2 is increased. With the same ratio of H_2 to O_2, the increase of $TiCl_4$ content contributes to the formation of rutile-TiO_2. With increasing the initial pressure of H_2-O_2 and retaining the $TiCl_4$ content, the formation of rutile-TiO_2 is increased.

3) The condition of detonation temperature of 2400~2600 K and detonation velocity of 2100~2200 m/s is conducive to the formation of anatase-TiO_2 when the half content of water vapor from reaction of H_2 and O_2 is more than or equal to the content of $TiCl_4$. When the half content of water vapor originating from reaction of H_2 and O_2 is less than the content of $TiCl_4$, the formation of rutile-TiO_2 is increased under the condition of detonation temperature of 3000~3500 K and detonation velocity of 1800~2000 m/s.

4) It is difficult to synthesize nano-TiO_2 with desired crystalline structure, i. e., the controllable accuracy of detonation reaction conditions and detonation parameters of GLD needs to be further verified.

References

1 Wu Q P, Huang F, Zhao M S *et al*. *Nano Energy*[J], 2016, 24: 63
2 Ding Q Q, Li R, Chen M D *et al*. *Applied Materials Today*[J], 2017, 9: 251
3 Djokić V R, Marinković A D, Petrović R D *et al*. *ACS Applied Materials & Interfaces*[J], 2020, 12(29): 33 058
4 Xie H Q, Chen M, Wu L M. *Small*[J], 2017, 13(22): 1 604 283
5 Xing Y L, Wang S B, Fang B Z *et al*. *Journal of Power Sources* [J], 2018, 385: 10
6 Hao Z K, Chen Q, Dai W R *et al*. *Advanced Energy Materials*[J], 2020, 10(10): 1 903 107
7 Zhang S, Zhao L J, Huang B Y *et al*. *Sensors and Actuators B: Chemical*[J], 2020, 319: 128 264
8 Raghu A V, Karuppanan K K, Pullithadathil B. *ACS Sensors*[J], 2018, 3(9): 1811
9 Alotaibi A M, Williamson B A, Sathasivam S *et al*. *ACS Applied Materials & Interfaces*[J], 2020, 12(13): 15 348
10 He Y, Huang G H, An C J *et al*. *Science of the Total Environment* [J], 2018, 616-617: 1628
11 Puma G L, Bono A, Krishnaiah D *et al*. *Journal of Hazardous Materials*[J], 2008, 157(2-3): 209
12 Lin X J, Sun M X, Gao B W *et al*. *Journal of Alloys and Compounds*[J], 2021, 850: 156 653
13 Wu S Y, Wang W J, Tu W G *et al*. *ACS Sustainable Chemistry & Engineering*[J], 2018, 6(11): 14 470
14 Chen C Y, Lin T C, Chuang W S *et al*. *Applied Surface Science* [J], 2020, 530: 147 204
15 Wang C, Qian C G, Liu J N *et al*. *Combustion and Flame*[J], 2018, 197: 400
16 Zhou F, Liu N, Zhang X Y. *International Journal of Hydrogen Energy*[J], 2018, 43(10): 5405
17 Xiang J Y, Luo N, Yan H H *et al*. *Rare Metal Materials and Engineering*[J], 2019, 48(10): 3113
18 Luo N, Jing H W, Ma Z G *et al*. *Particuology*[J], 2016, 26: 102
19 Luo N, Shen H, Jing H W *et al*. *Particuology*[J], 2017, 35: 78
20 Wu L S, Yan H H, Xiao J L *et al*. *Ceramics International*[J], 2017, 43(16): 14 334

21 Wu L S, Yan H H, Li X J *et al*. *Ceramics International*[J], 2016, 43(1B): 1517
22 Barin I, Platzki G. *Thermochemical Data of Pure Substances* [M]. Weinheim: VCh, 1989
23 Hu Shuangqi. *Combustion and Explosion*[M]. Beijing: Beijing Institute of Technology Press, 2015 (in Chinese)
24 Spurr R A, Myers H. *Analytical Chemistry*[J], 1957, 29(5): 760
25 Guo D Z, An Q. *ACS Applied Materials & Interfaces*[J], 2018, 11(1): 1512
26 Zhu K R, Zhang M S, Hong J M *et al*. *Materials Science and Engineering A*[J], 2005, 403(1-2): 87
27 Sabyrov K, Burrows N D, Penn R L. *Chemistry of Materials*[J], 2013, 25(8): 1408
28 Zhao T J, Yan H H, Li X J *et al*. *Phase Transitions*[J], 2017, 90(6): 618
29 Hanaor D A, Sorrell C C. *Journal of Materials Science*[J], 2011, 46(4): 855
30 Chaturvedi A, Joshi M P, Mondal P *et al*. *Applied Surface Science*[J], 2017, 396: 303
31 Manna A, Barman A, Joshi S R *et al*. *Journal of Applied Physics* [J], 2018, 124(15): 155 303

气液爆轰控制合成多晶纳米二氧化钛

罗　宁[1,2,3]，孙　鑫[1,2,3]，范学如[1,2]，梁汉良[1,2,3]，陈彦龙[1,2]，张桂民[1,2]，董纪伟[1,2]，翟　成[4]

(1. 中国矿业大学 力学与土木工程学院，江苏 徐州 221116)

(2. 中国矿业大学 深部岩土力学与地下工程国家重点实验室，江苏 徐州 221116)

(3. 中国矿业大学 爆炸力学与工程爆破研究中心，江苏 徐州 221116)

(4. 中国矿业大学 安全工程学院，江苏 徐州 221116)

摘　要：以氢气、氧气和四氯化钛为混合前驱体，通过气液爆轰法合成了多晶纳米二氧化钛。研究了不同摩尔比例的前驱体和初始反应压力对纳米二氧化钛晶相结构的影响。采用X射线衍射及透射电子显微镜对产物的纳米结构、成分、颗粒大小和形态进行了表征。结果表明：获得的二氧化钛存在纯净的锐钛矿相、纯净的金红石相和混合相，其中混合相的球形或者类球形颗粒粒径为20~150 nm。分析了纳米二氧化钛在气液爆轰中的形成机制。基于C-J理论和化学反应数据，计算了爆轰参数；该参数验证了不同摩尔比例的前驱体和初始反应压力对控制合成多晶纳米二氧化钛的影响。

关键词：纳米二氧化钛；气液爆轰；多晶纳米结构；爆轰参数；C-J理论

作者简介：罗　宁，男，1980年生，博士，教授，中国矿业大学力学与土木工程学院，江苏 徐州 221116，E-mail：nluo@cumt.edu.cn